LHI Journal
of Land, Housing, and Urban Affairs

pISSN: 2093-8829, eISSN: 2234-1765
LHI Journal 2020;11(2):87-94 • http://doi.org/10.5804/LHIJ.2020.11.2.87

Simplified Limit Solutions for the Inclined Load Capacity of a Dynamically Installed Pile in Soft Clay

Junho Lee* · **Jong-Suk Jung**** · **Young-Jong Sim***** · **Yong-Boo Park******

Abstract

Offshore renewable energy resources are attractive alternatives in addressing the nation's clean energy policies because of the high demand for electricity in the coastal region. As a large portion of potential resources is in deep and farther water, economically competitive floating systems have been developed. Despite the advancement of floating technologies, the high capital cost remains a primary barrier to go ahead offshore renewable energy projects. The dynamically installed piles (DIPs) have been considered one of the most economical pile concepts due to their simple installation method, resulting in cost and time-saving. Nevertheless, applications to real fields are limited because of uncertainties and underestimated load capacity. Thus, this study suggests the appropriate analytical approach to estimate the inclined load capacity of the DIPs by using the upper bound plastic limit analysis (PLA) method. The validity of the PLA under several conditions is demonstrated through comparison to the finite element (FE) method. The PLA was performed to understand how flukes, soil profiles, and load inclinations can affect the inclined load capacity and to provide reliable evaluations of the total resistance of the DIPs. The studies show that PLA can be a useful framework for evaluating the inclined load capacity of the DIPs under undrained conditions.

Keywords: Plastic Limit Analysis, Dynamically Installed Pile, Inclined Loading, Offshore Foundations

1. Introduction

Much of renewable energy facilities such as offshore wind or wave are located at deep and farther water due to stronger and more consistent resources. As development progresses deeper water, the capital costs of the fixed structure increase exponentially. The floating system moored anchors or piles on the seabed is a cost-effective alternative. Despite the improvement of the floating technologies, high capital costs for securing floating structures remains a primary obstacle. Thus, the floating system requires cost-effective anchors to make it economically competitive. The dynamically installed piles (DIPs) have proven to be a robust alternative in the offshore fields (Medeiros, 2002; Brandão et al., 2006). Since the DIPs are typically rocket-shaped with up to four flukes, they sometimes termed "torpedo anchors". They are penetrated into the seabed by free fall and their own weight as kinematic driving energy. The DIPs are typically a diameter of 0.8-1.2 m, 12-17 m long with dry unit weight in the range of 230-1150 kN (Brandão et al., 2006; Randolph et al., 2011). They can have significant

* Ph.D. Candidate, Civil & Environmental Engineering, Texas A&M University (juno918@tamu.edu)
** Researcher, Land & Housing Institute
*** Researcher, Land & Housing Institute
**** Senior Researcher, Land & Housing Institute (Corresponding author: parkyb@lh.or.kr)

(**Received:** April 2, 2020 / **Revised:** July 17, 2020 / **Accepted:** July 20, 2020)

advantages of quick, economical installation. They can be installed in normally consolidated clay, overconsolidated clay, sand, and calcareous deposits (Ehlers et al., 2004). The loading directions on the moored anchors vary from vertical (tension leg platform) to horizontal (catenary), including inclined (taut) loading. The catenary moorings require excessive lateral distance in deep water, resulting in space and cost consuming compared to taut moorings. Hence, the taut mooring system becomes a more attractive alternative in deep water. Despite the importance of taut mooring in offshore applications, the estimation of the inclined load capacity of a DIP remains a significant challenge. (O'Loughlin et al., 2004; 2009) and Richardson et al. (2009) focused on centrifuge tests to investigate the vertical load capacity. de Sousa et al. (2011) and Kim and Hossain (2016) carried out large-deformation FE (LDFE) analyses to estimate the inclined load capacity. They adopted enhanced strain theory and coupled Eulerian-Lagrangian approach to avoid element distortion from large deformation. However, these retain much of rigor of a more complex numerical approach and much computational efforts. Table 1 indicates that a plastic limit approach for estimating the load capacity of DIPs is more efficient than FE in terms of computational efficiency.

Therefore, this study presents a simple plastic limit approach and estimate the effects of various factors on the inclined load capacity of DIPs. The formulation considers the inclined resistance of flukes, vertical, and moment resistance at the top of the embedded piles. This approach can provide a relatively simple and efficient analysis method accessible to practicing engineers compared to FE methods.

Table 1. The computational efficiency of FE and PLA for a typical pile in soft clay

Scenarios		FE (using ABAQUS)	PLA (using MATLAB)	Comments
Estimating F_h, F_v, F_{total} at L_{iopt}	T	CM: 0.3 hrs/wrk MM: 6 hrs/wrk FM: 12 hrs/wrk	1 sec for 100 wrks	–
	MEM	CM: 0.4 GB/wrk MM: 4 GB/wrk FM: 9 GB/wrk	1.4 GB	
Estimating L_{iopt} under F_v	T	(for 10 wrks) SIM: 6 hrs SEQ: 60 hrs	1.5 sec for 120 wrks	MM was used for FE analyses
	MEM	40 GB for 10 wrks, regardless of SIM and SEQ	1.4 GB	
Estimating L_{iopt} under combined loading	T	(for 10 wrks) SIM: 6 hrs SEQ: 60 hrs	190 sec for 120 wrks	Refer to Fig. 4 (10 FE values =10 wrks)
	MEM	40 GB for 10 wrks, regardless of SIM and SEQ	1.4 GB	

Abbreviations: T, calculation time; MEM, required memory; CM, coarse mesh; MM, medium mesh; FM, fine mesh; hrs, hours; wrk, iteration work; SIM, simultaneous work; SEQ, sequential work.

2. Modifications of PLA for DIPs

2.1 PLA for conventional piles

The plastic limit analysis (PLA) methods provide an evaluation of a collapse load for the piles or anchors. A plastic limit approach to the horizontal load capacity of piles was first proposed by Murff and Hamilton (1993). They derive dissipation functions and lateral bearing capacity factor N_{ps} based on von Mises and Tresca yield criteria and an associated flow rule. Aubeny et al. (2001; 2003) proposed a simplified upper bound model. They also derive energy dissipation functions, relationships for lateral-axial bearing capacity factor N_{ps}-N_{as} on the side of the pile, and interaction among ultimate resistance to vertical, horizontal and moment loading at the bottom of the pile. All of the studies above are limited to consider a simple cylinder shape. In contrast, a DIP has flukes resulting in different failure mechanisms compared to conventional piles or caissons. In order to evaluate the load capacity of the DIP using the PLA method, there is a need to consider specific conditions of DIPs such as flukes and deep embedment depth.

2.2 Key issues for modifications

Due to different geometry of the DIPs compared to the conventional pile, the analysis of the DIPs needs some modifications from the conventional pile analyses. Firstly, since the DIP installed in deep depth, there is resistance at the top of the anchor. This leads to apply the formulation for lateral-mo-

ment resistance at the bottom of piles described by Aubeny (2017) into the top of the DIP. Secondly, the bearing resistance from the flukes requires to be considered to the overall lateral capacity. Lee and Aubeny (2019) quantified this mechanism of resistance and suggested the lateral bearing factors considering various conditions. Thus, FE calculated bearing factors are adopted in the current study. The selected bearing factor N_{ps} for the fluke-cylinder zone is about 11.42, which is slightly conservative. Preliminary findings show the value of N_{ps} can vary depending on the width of flukes, the total number of flukes, and load angles. N_{ps}, which considers the effect of the flukes on a DIP, was applied to the following equations.

For side axial-lateral interaction,

$$N_{ps} \le I_3 R_f, f_s = N_{as} - \pi\alpha = 0 \tag{1}$$

$$N_{ps} \le I_3 R_f, f_s = (N_{ps} - I_3 R_f)^2 + (R_f N_{as})^2 / I_1 - I_2 R_f^2 = 0 \tag{2}$$

where f_s is the side resistance, N_{as} is the axial side resistance factor, N_{ps} is the lateral side resistance factor, I_1, I_2, I_3, and R_f are curve fitting coefficient for N_{as}-N_{ps} interaction relation, and α is the adhesion factor.

For end axial-moment interaction,

$$f = \left(\frac{V}{V_{max}}\right)^2 + \left(\frac{M}{M_{max}}\right)^2 - 1 = 0 \tag{3}$$

$$\text{at tip, } M_b = \left[2\left(\frac{R_1}{\pi R}\right) + \exp\left(\frac{-I_4 R_1}{R}\right)\right]\left(\frac{\pi^2 R^3 s_{ub}}{2}\right) \tag{4}$$

$$\text{at top, } M_t = \left[2\left(\frac{R_3}{\pi R}\right) + \exp\left(\frac{-I_4 R_3}{R}\right)\right]\left(\frac{\pi^2 R^3 s_{ut}}{2}\right) \tag{5}$$

$$M = M_b + M_t \tag{6}$$

where M_t is the mobilized moment resistance at the top of the pile, M_b is the mobilized moment resistance at the bottom of the pile, R is the pile radius, R_1 is the distance from the center of rotation to pile tip (=L-L_0), R_3 is the distance from the center of rotation to pile top (=L-R_1), R_2 and R_4 are the radii of spherical surface at the top and tip respectively (Fig. 1),

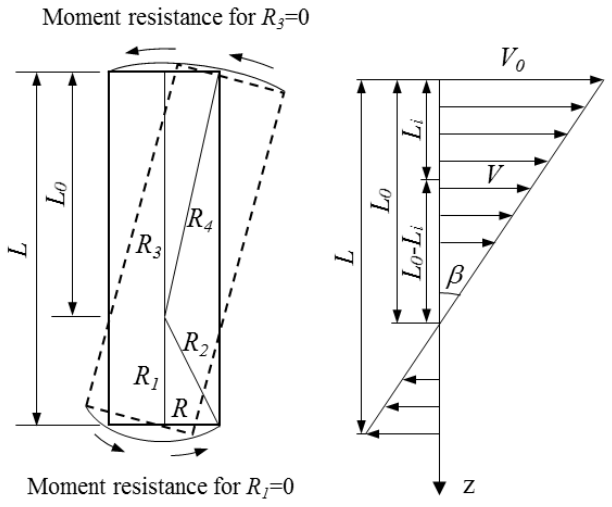

Fig. 1. The schematic diagram for moment resistances

I_4=1.118, the coefficient of curve fitting, s_{ut} and s_{ub} are respectively the undrained shear strengths at the top and tip, and M is the total moment resistance at top and base of the pile.

$$V_0 = V_{b0} + V_{t0} = N_{ab}\pi R^2 s_{ub} + N_c \pi R^2 s_{ut} \tag{7}$$

where V_0 is total uplift capacity under pure vertical loading, V_{b0} is uplift capacity under vertical loading at the bottom of the pile, V_{t0} is uplift capacity under vertical loading at the top of the pile, N_c is the end beating foactor at the top (assumed N_c=9 for an annular tip, and N_c=7.5 for flukes), and N_{ab} is the reverse end bearing factor, typically varying 9 to 12 (Aubeny 2017).

The internal energy dissipation from the soil resistance in unit length on the side (F_{as}=$N_{as}s_uD$, F_{ls}=$N_{ps}s_uD$) and from the base and top (V, M) can be equated to the external work as follows:

$$H = \frac{\int\left(F_{ls}\left|1 - \frac{z}{L_0}\right|\right)dz + \frac{M}{L_0} + V\xi}{\left(\xi\tan\theta + \left|1 - \frac{L_i}{L_0}\right|\right)} \tag{8}$$

$$V = H\tan\theta \tag{9}$$

where H and V are respectively horizontal and vertical load capacity of the pile, z is the depth below mudline, ξ is the optimization parameter controlling the vertical velocity of the pile,

L_i is the load attachment depth, and L_0 is the center of rotation.

The procedure of a typical upper bound PLA solution is as follows: through a postulated kinematically admissible collapse mechanism, the external virtual work and the virtual rate of internal energy dissipation are calculated. Then, equating both of it to obtain the collapse load (Aubeny, 2017). If the externally applied force is inclined at load angle θ, the axial and lateral components are related by $\tan\theta=V/H$. Thus, V can be calculated by the simple expression after computing H.

2.3 Validations

The modified PLA model is validated through comparison to FE analysis and field data indicated in Table 2 and Figs. 2-4. Medeiros (2002) conducted several load tests in normally consolidated clay (s_u=5+2z) in the Campos basin area. Two torpedo anchors without flukes are used to evaluate the pull-out capacity. Numerical investigations were carried out by de Sousa et al. (2011) to estimate the ultimate inclined load capacity

Table 2. Validation of a modified PLA through comparison to field data and FE results

Descriptions		Reference data (RD)	PLA	|RD-PLA| / PLA	Ref. Fig.
Considerations	Variables				
Different soil profiles	s_u=1.5z	5.2-6.6 MN	5.2-7.3 MN	0.7-8.6%	Fig.2
	s_u=3z	7.7-12.3 MN	7.7-12.5 MN	0.4-7.0%	
	s_u=6z	11.5-21.6 MN	11.6-21.3 MN	1.3-8.4%	
	3-D FE computed values (de Sousa et al, 2011) D: 1.1 m, L: 17.2 m, 4 flukes (W_f:0.9 m)				
Effects of W_f and L_{iopt}	W_f=0.1 m	1.7-4.6 MN	1.6-4.4 MN	3.7-10.4%	Fig.3
	W_f=0.38 m	2.4-6.7 MN	2.3-6.6 MN	0.1-5.6%	
	W_f=0.84 m	3.4-10.0 MN	3.5-10.0 MN	0.1-2.9%	
	3-D FE computed values (this study) D: 0.76 m, L: 12 m, 4 flukes, s_u=5+2z				
Instant pull-out capacity	D=0.76 m	0.9-1.1 MN	around 1.1 MN	0-0.5%	Fig.4
	D=1.07 m	1.9-2.1 MN	1.9-2.2 MN	0-2.5%	
	Field data (Medeiros, 2002) L: 12 m, no flukes, s_u=5+2z				

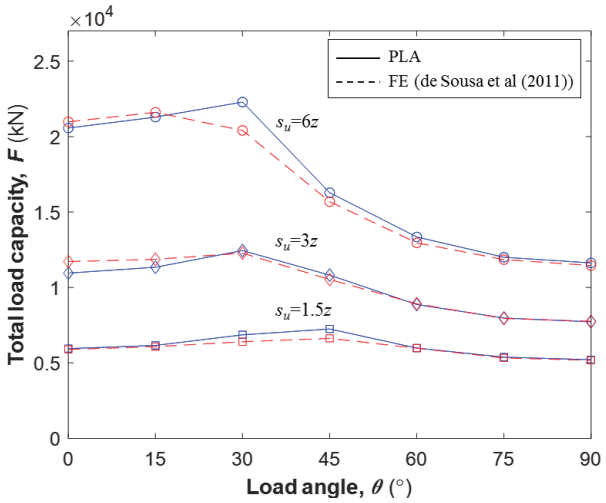

Fig. 2. Comparison between PLA and FE: the effect of soil profile on total load capacity (de Sousa et al. (2011))

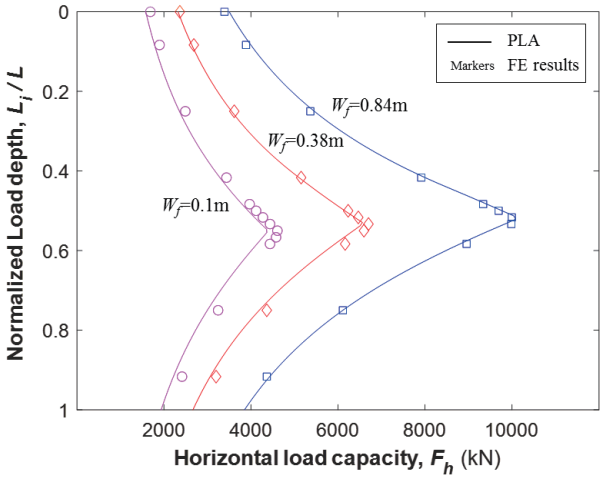

Fig. 3. Comparison between PLA and FE: the effects of the width of flukes and load attachment depth on horizontal load capacity

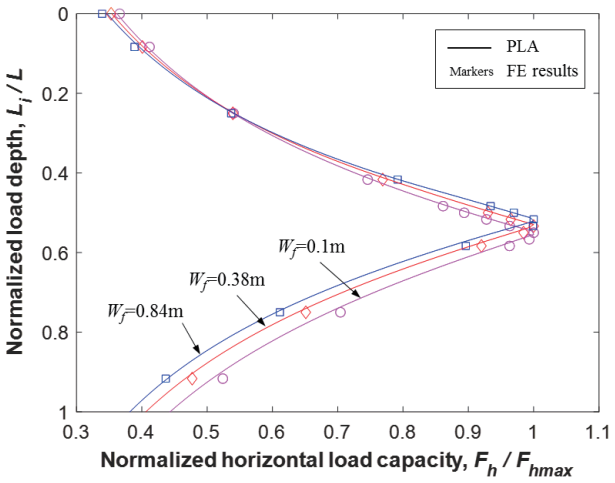

Fig. 4. Comparison between PLA and FE: the trend of the normalized curve, L_i/L–F_h/F_{hmax}

under different undrained shear strength. In this study, three dimensional FE analyses were also performed using Abaqus/Standard to understand the effect of various parameters on total load capacity. The soil model considered as linearly elastic-perfectly behavior beneath a Tresca yield criterion and associated flow. To simulate the undrained loading condition, a Poisson's ratio assumed μ=0.49. Young's modulus was also assumed as a ratio E/s_u=500, which does not affect the ultimate load capacity (Aubeny, 2017).

Table 2 indicates that the computed PLA results fit within the range of in-situ measured data. The previous FE study, which estimated ultimate load capacity under various soils profiles and load inclinations, matches well with PLA results (Fig. 2, de Sousa et al. (2011)). The characterization of the optimum depth of load attachment using PLA is consistent with the results of FE analyses as shown in Fig. 3. Even though displacement-based FE analyses tend to overestimate collapse load by about 10 percent, the trends of FE calculated values such as normalized curve L_i/L-F_h/F_{hmax} matches well with the trend of PLA values (Fig. 4). These reasonable consistencies confirm the capability of a modified PLA model in assessing the ultimate load capacity of DIPs under various conditions.

3. Parametric Study

In order to understand the effect of flukes, soil profiles, load attachment depth, and load inclination on the DIP in soft clay, the current study evaluated the following parameters.

- Width of the flukes, W_f
- Undrained shear strength of the soil, s_u
- Load attachment depth from the top of the pile, L_i
- Load inclination of mooring line at the top, θ

The DIP dimensions were from field data (Medeiros, 2002) to evaluate the DIP performance in soft clay. The DIP equipped with four flukes has used a diameter of 0.76 m, a length of 12 m, and a tip embedment depth of 20 m (Fig. 5). The width of the flukes varies from 0 m (no fluke) to 0.9m. In all analyses, seven load inclination θ with respect to the horizontal direction were considered: 0° (lateral load), 15°, 30°, 45°, 60°, 75°, and 90° (axial load). Additionally, all range of load attachment depth L_i will also be considered to investigate the effect of load attachment depth. The soil profile has a typical soft clay that has an undrained shear strength at the seabed s_{u0}=5 kPa and linear strength gradient s_{u1}=2 kPa/m, as the same values from Medeiros (2002). The submerged self-weight of soil is assumed as 6 kN/m^3.

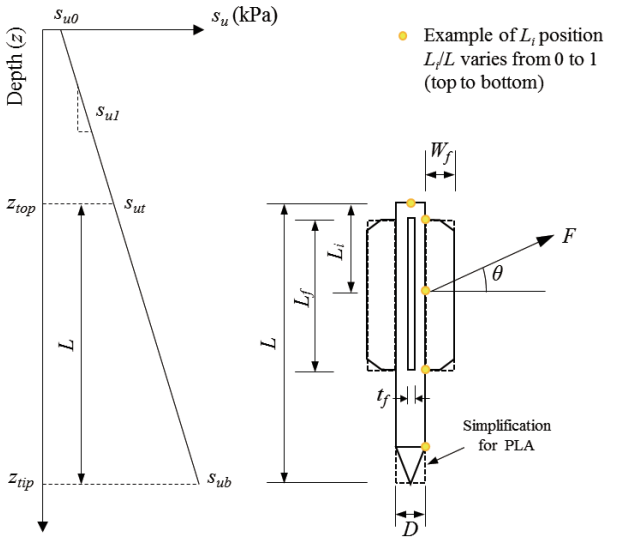

Fig. 5. The schematic diagram of DIP

In the current study, three different undrained shear strengths were assumed, s_u=1.5z, s_u=3z, and s_u=6z, to understand the effect of undrained shear strength on the DIPs. Soil-Pile adhesion factors were calculated by the well-established formulas proposed by API (2005) as follows:

$$\Psi(z)\le 1.0, \alpha(z)=0.5\Psi(z)^{-0.5} \tag{10}$$

$$\Psi(z)>1.0, \alpha(z)=0.5\Psi(z)^{-0.25} \tag{11}$$

where $\psi(z)=s_u(z)/P_0(z)$, and P_0 is the effective overburden pressure.

4. Analyses and Results

4.1 The optimum load attachment depth

The trends between load capacity and the effect of load attachment depth are illustrated in Fig. 6. For lower inclinations (between 0° and 15°), the maximum load capacity perfectly positioned at the optimal load attachment depth. Fig. 7 also shows that the normalized load capacity F/F_{max} for

lower inclinations is highly sensitive to load attachment depth. However, for higher inclination (over 45°), the maxim load capacity can be calculated over a relatively wide range of load attachment depths as shown in Figs. 6–7. It is worth mentioning that a DIP had the maximum resistance when the lower inclined load applied at the optimal attachment depth.

4.2 Effect of the width of the flukes

Fig. 8 presents that inclined load capacities are affected by the width of the flukes. While reduction from W_f=0.9 m to 0 m (no fluke), the reductions of total lateral contact area are 35% (from 0.9 to 0.45 m), 58% (from 0.9 to 0.15 m), finally 69% (from 0.9 to no fluke). These reductions of lateral contact areas may affect load capacity, resulting in the reductions of horizontal load capacity are 48%, 62%, and 71%, respectively. From these results, the total contact area of the pile seems to be an important parameter to evaluate the load capacity. Fig. 9 illustrates the effect of the width of flukes on the inclined load capacity interaction diagram. The horizontal components of load capacity for load inclination below 30° are close to horizontal load capacity. On the contrary, the vertical components for higher load inclination are almost the same as vertical load.

4.3 Effect of Undrained Shear Strength

The increase in the undrained shear strength affects an increase in the load capacity of the pile (Fig. 10). The increase

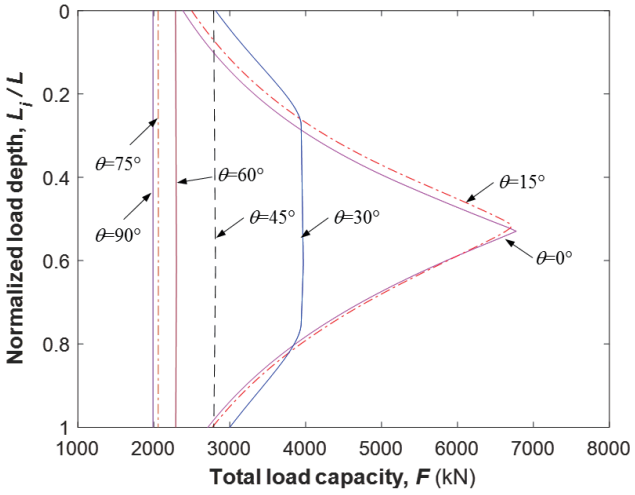

Fig. 6. Effect of load attachment depth and load angle on total load capacity

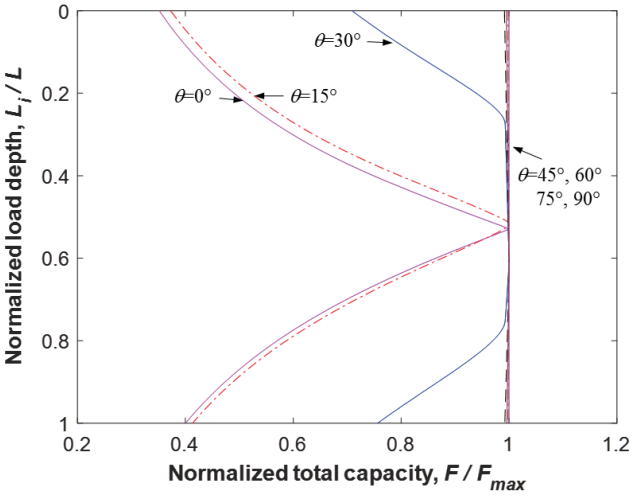

Fig. 7. The trend of the normalized curve L_i/L–F/F_{max}

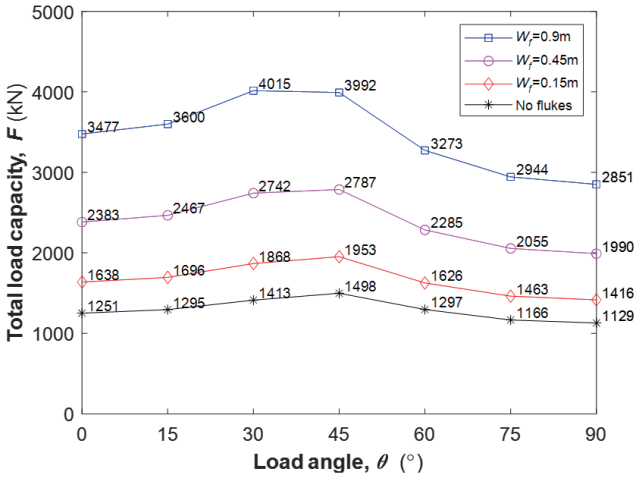

Fig. 8. Effects of the width of the flukes and load angle on total load capacity

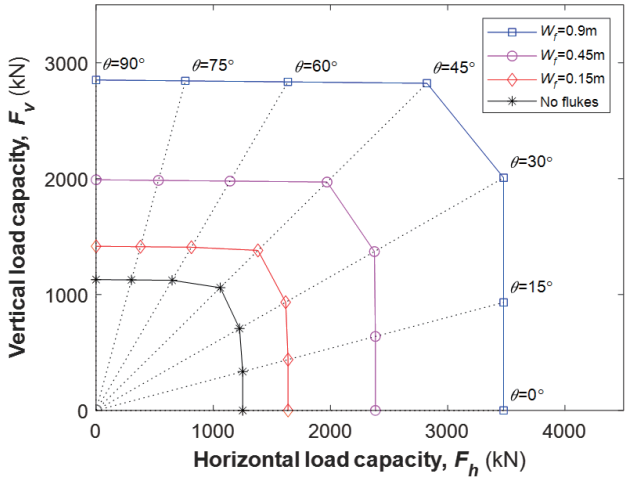

Fig. 9. Effects of the width of the flukes and load angle on horizontal and vertical load capacity

for lower load inclinations, between 0° and 30°, is higher than that for higher load inclinations, between 60° and 90°. Under higher inclination, the adhesion factor α affects to reduce the shear stress between pile and soil. The load capacity under higher load inclination is highly affected by the adhesion characteristics between pile and soil.

When s_u equals to 1.5z, the maximum value occurs about θ=45°. The load capacity increase with the load inclination until the maximum load capacity and decrease after 45°. This trend is similarly shown in other soil conditions. However, the angles at which the maximum value occurs are different depending on soil profiles such as s_u=3z and s_u=6z, respectively. As an example of this, the maximum load under s_u=6z capacities occur when the load inclinations are close to 30°. Fig. 11 illustrates the effect of the undrained shear strength on the inclined load capacity interaction diagram. The results of this analysis are having similar trends mentioned above. Horizontal components of load capacity for load inclination below 30° are close to horizontal load capacity, while the vertical components for higher load inclination are almost the same as vertical load.

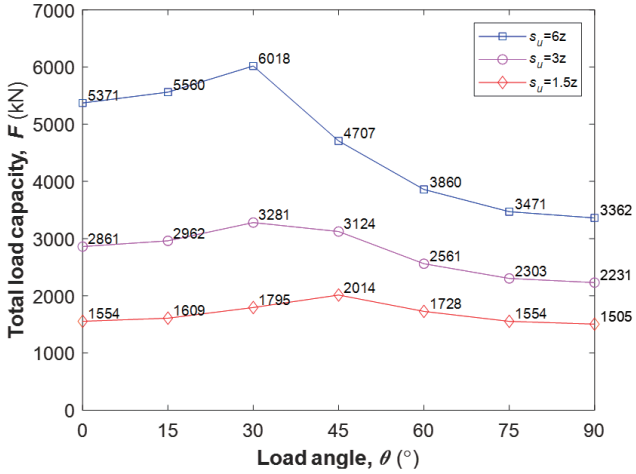

Fig. 10. Effect of soil profile and load angle on total load capacity

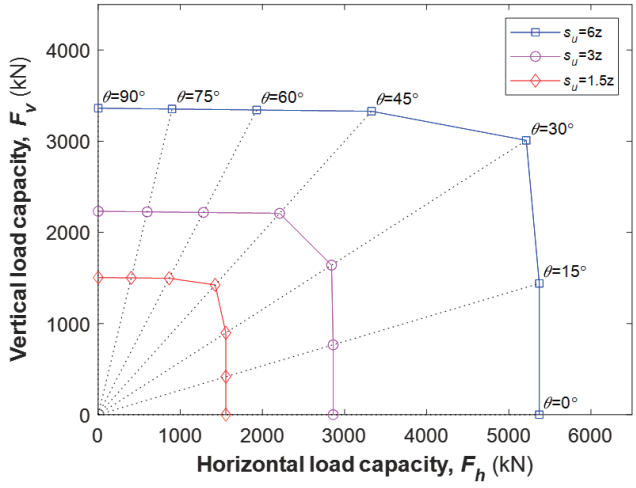

Fig. 11. Effect of soil profile and load angle on horizontal and vertical load capacity

5. Concluding Remarks

This study presents a computational-effective plastic limit approach for DIPs considering the effects of the flukes and deep embedment depth. For these reasons, the PLA can be an attractive design tool for practicing engineers. A parametric study represents the effect of load attachment depth L_i, angle of load inclination θ, the width of the flukes W_f, and undrained shear strength of soil s_u on the load capacity of the DIPs. The basic findings are as follows:

- For the lower angle of load inclination (less than 30°), The load capacity is very sensitive to load attachment depth. On the contrary, load capacity becomes less sensitive to load attachment depth at larger load inclination (more than 45°).
- The total contact area of piles and the soil profile seem to be important parameters to estimate the ultimate load capacity. Consequently, the increase of the width of the flukes and undrained shear strength significantly increase the load capacity of the DIP.
- Quantifying the lateral-moment interaction at the top and bottom of the pile is required to better understand the DIP performance in soft clay better. This has been identified as a future research need.

Nomenclature

D	Diameter of the shaft of DIP
F	total load capacity
F_{max}	maximum total load capacity
F_h, F_v	horizontal and vertical load capacity
L	length of the pile
L_i	load attachment depth from the top of the pile
L_{iopt}	optimum load attachment depth

L_0	center of rotation of pile
L_f	length of fluke
n	number of flukes
N_{as} N_{ps}	axial & lateral resistance factor on the side of a pile
N_{af} N_{pf}	axial & lateral resistance factor on the side of the fluke
S_t	soil sensitivity
s_u	undrained shear strength of the soil
s_{u0}	undrained shear strength at mudline
s_{u1}	rate of strength increase per unit length
s_{ub}	undrained shear strength at the base
s_{ut}	undrained shear strength at the top
t	thickness of the pile
t_f	thickness of fluke
u	displacement of the pile at the load attachment depth
W_f	width of fluke
z	depth below mudline
z_{tip}	pile tip embedment depth
z_{top}	pile top embedment depth

Greek Letters

α	adhesion factor
θ	angle of load inclination from horizontal
ψ	dilation angle of the soil

References

1. API (2005), "Recommended Practice for Planning, Designing and Constructing Fixed Offshore Platforms", Washington, D.C: American Petroleum Institute.
2. Aubeny, C. (2017), *Geomechanics of Marine Anchors*, CRC Press, Taylor & Francis Group, Boca Raton.
3. Aubeny, C., Murf, J., and Moon, S. (2001), "Lateral undrained resistance of suction caisson anchors", *International Journal of Offshore and Polar Engineering*, 11(03).
4. Aubeny, C. P., Han, S. W., and Murff, J. D. (2003), "Inclined load capacity of suction caissons", *International Journal for Numerical and Analytical Methods in Geomechanics*, 27(14): 1235-1254.
5. Brandão, F., Henriques, C., Araújo, J., Ferreira, O., and dos Santos Amaral, C. (2006), "Albacora leste field development-FPSO P-50 mooring system concept and installation", *Proc., Offshore Technology Conference*, Offshore Technology Conference.
6. de Sousa, J. R. M., de Aguiar, C. S., Ellwanger, G. B., Porto, E. C., Foppa, D., and de Medeiros, C. J. (2011), "Undrained load capacity of torpedo anchors embedded in cohesive soils", *Journal of Offshore Mechanics and Arctic Engineering*, 133(2): 021102.
7. Ehlers, C. J., Young, A. G., and Chen, J. H. (2004), "Technology assessment of deepwater anchors", *Proc., Offshore Technology Conference*, Offshore Technology Conference.
8. Kim, Y. and Hossain, M. (2016), "Numerical study on pull-out capacity of torpedo anchors in clay", *Géotechnique Letters*, 6(4): 275-282.
9. Lee, J. and Aubeny, C. P. (2019), "Effect of wing plates on a multiline ring anchor system in cohesive soils", *Proc., OCEANS 2019 MTS/IEEE SEATTLE*, 1-6.
10. Medeiros, C. J., Jr. (2002), "Low cost anchor system for flexible risers in deep waters", *Proc., Offshore Technology Conference*, Offshore Technology Conference, Houston, Texas, 5.
11. Murff, J. D. and Hamilton, J. M. (1993), "P-Ultimate for Undrained Analysis of Laterally Loaded Piles", *Journal of Geotechnical Engineering*, 119(1): 91-107.
12. O'Loughlin, C. D., Randolph, M. F., and Richardson, M. (2004), "Experimental and theoretical studies of deep penetrating anchors", *Proc., Offshore Technology Conference*, Offshore Technology Conference, Houston, Texas.
13. O'Loughlin, C. D., Richardson, M. D., and Randolph, M. F. (2009), "Centrifuge tests on dynamically installed anchors", *International Conference on Offshore Mechanics and Arctic Engineering*, 43475, 391-399.
14. Randolph, M. F., Gaudin, C., Gourvenec, S. M., White, D. J., Boylan, N., and Cassidy, M. J. (2011), "Recent advances in offshore geotechnics for deep water oil and gas developments", *Ocean Engineering*, 38(7): 818-834.
15. Richardson, M., O'Loughlin, C., Randolph, M., and Gaudin, C. (2009), "Setup following installation of dynamic anchors in normally consolidated clay", *Journal of Geotechnical and Geoenvironmental Engineering*, 135(4): 487-496.